# FITTING METHOD OF SPINNING PROJECTILE TRI-ORTHOGONAL GEOMAGNETIC OUTPUT BASED ON IMPROVED PARTICLE SWARM OPTIMIZATION ALGORITHM

**Zilu He[1], Yiji Liu[1], Qi Liang[1], Yundong He[1], Xin Chen[1], Xiongzhu Bu[2], Miaomiao Xu[3]**

*1) Shanghai Electro-Mechanical Engineering Institute, Shanghai, China*
*2) Nanjing University of Science and Technology, School of Mechanical Engineering, Nanjing, China*
    (✉ *buxu105@njust.edu.cn*)
*3) Nantong University, School of Information Science and Technology, Nantong, China*

**Abstract**

Obtaining the characteristics at a characteristic point of the outputs is a key step to the geomagnetic attitude measurement method of the spinning projectile. However, actual outputs usually have some noise that causes the characteristic points to deviate from the theoretical position or produce multiple fake characteristic points, resulting in the increase of solution error and even the failure of solution. In addition, the coning motion and inaccurate initial alignment of the spinning projectile increase the number of unknown parameters and the computational complexity. In this study, several improved particle swarm optimization strategies are proposed. The actual outputs are fitted to the geomagnetic output equations under the coning motion, and the supervised learning effect of each strategy is analysed and compared. The algorithm can be flexibly adjusted according to different needs in actual use by selecting appropriate strategies, which has a wide applicability in data fitting.

Keywords: improved particle swarm optimization, geomagnetic attitude measurement, coarse initial parameter, weak boundary condition.

## 1. Introduction

Due to its high-speed rotation, the spinning projectile has a high stability during flight and has become a widely used conventional weapon. In order to improve the hit accuracy of the spinning projectile fired by conventional artillery, many researchers have carried out studies on measurement method of its attitude. With the development of MEMS magnetic sensors, the geomagnetic attitude measurement method has the advantages of miniaturization, low cost and low power consumption while meeting the requirements of all-time and all-weather autonomous attitude measurement, and has become one of the rapidly developed attitude measurement methods in recent years. However, as the three output equations of the tri-orthogonal magnetic sensor are

not independent of each other, it is unable to solve the full attitude angles. It can only be used as an auxiliary method to integrate with other attitude measurement methods such as inertial attitude measurement, infrared attitude measurement and so on [1, 2]. In order to overcome this problem, some scientific researchers have designed algorithms which can independently solve the full attitude angles of the spinning projectile through the characteristics of the geomagnetic outputs such as the zero-crossing method [3], the cross-ratio method [4], the integral ratio method [5], and the derivative ratio method [6]. However, most of these algorithms are based on the ideal state in which the noise is very low. In this case, key parameters such as frequency and amplitude can be easily obtained according to the statistical regularity of noise and simple data processing such as FFT. Moreover, in most of these algorithms, the forward direction of the spinning projectile is regarded as always consistent with the tangent direction of the trajectory, and the coning motion of the spinning projectile due to the Magnus effect is ignored [7–9]. As a result, it is difficult to estimate the coning motion frequency and taper angle of the spinning projectile by traditional data processing methods. In addition, in practical applications, sometimes the initial state of the spinning projectile can only be obtained through rough alignment, so it is more difficult to estimate the geomagnetic output parameters. Therefore, it is necessary to propose a method that can accurately obtain the initial attitude angles, taper angle, spinning speed and coning motion frequency of the spinning projectile at the same time, so as to provide signal characteristics for the geomagnetic measurement method of the spinning projectile.

In view of the key parameters of the geomagnetic field and the motion characteristics of the spinning projectile, Li *et al.* established an attitude measurement model of the three-axis magnetic sensor of the spinning projectile [10]. On this basis, He *et al.* established a geomagnetic measurement model of spinning projectile under coning motion [6], providing a standard for calibrating geomagnetic characteristic parameters through data fitting. The actual output signals are inevitably be mixed with a certain degree of noise, which will affect the result of data fitting. In the calibration of magnetic sensors, Yu *et al.* calibrated an AC vector magnetometer with the ellipse fitting method [11]. Li *et al.* designed a least squares regression algorithm that can realize online calibration [12]. Sun *et al.* studied the error compensation method of ellipse fitting calibration of a magnetometer [13]. Li *et al.* proposed a dual inner product method to improve the calibration and alignment of the magnetometer [14]. Farhangian *et al.* fused the data of multiple magnetic sensors through UKF to accurately estimate the calibration parameters [15]. Crissidis *et al.* performed the calibration of magnetometers static errors with different dimensions based on the total least squares method [16]. The methods in [11–16] calibrate magnetic sensors to eliminate static and dynamic errors, enabling the sensors to output more accurate signals. However, when solving the attitude angles using the tri-orthogonal geomagnetic model, the geomagnetic signals will inevitably be coupled with noise. In order to eliminate the influence of noise, it is necessary to select appropriate optimization algorithms for processing geomagnetic signals.

Lu applied the gradient descent method to an inertial/geomagnetic navigation system and obtained the magnetic distortion parameters [17]. Zhou *et al.* adopted an improved iterative Gauss-Newton method to identify the aerodynamic parameters of high-spinning projectiles using GPS and geomagnetic measurement data [18]. Deng *et al.* introduced *backpropagation* (BP) neural networks to solve the inertial/geomagnetic attitude coupling model, reducing the root mean square error of attitude by more than 50% [19]. Cuenca *et al.* identified and described important contributors to the total magnetic field through deep learning and Gaussian regression processes to overcome interference and noise [20]. Among the above optimization algorithms, the gradient descent method has a low convergence speed, poor stability, and is highly sensitive to initial conditions. The Gauss-Newton method may generate ill-conditioned matrices during the solving process, resulting in incorrect results. The BP algorithm and deep learning can achieve

high-precision results when there is a large amount of data available for learning. However, as the flight time of conventional spinning projectile is limited, the amount of data available is not enough and there are many parameters to be estimated. Therefore, a relatively simple algorithm is needed to obtain all the required attitude measurement model parameters.

## 2. Measurement model of tri-orthogonal magnetic sensor

The principle of the tri-orthogonal geomagnetic attitude measurement method of the spinning projectile is to obtain one of the attitude angles according to some characteristics at a certain position of the magnetic outputs. The other two attitude angles are solved by using the tri-orthogonal geomagnetic equations. In [6], there are provided tri-orthogonal geomagnetic equations, as shown in (1) and (2)

$$
\begin{cases}
M_{sx0} = M_H \cos\psi_0 \cos\theta_0 - M_V \cos\psi_0 \sin\theta_0 \\
M_{sy0} = M_H(\sin\gamma_0 \sin\theta_0 - \cos\gamma_0 \sin\psi_0 \cos\theta_0) + M_V(\sin\gamma_0 \cos\theta_0 + \cos\gamma_0 \sin\psi_0 \sin\theta_0) , \\
M_{sz0} = M_H(\cos\gamma_0 \sin\theta_0 + \sin\gamma_0 \sin\psi_0 \cos\theta_0) + M_V(\cos\gamma_0 \cos\theta_0 - \sin\gamma_0 \sin\psi_0 \sin\theta_0)
\end{cases}
\tag{1}
$$

where $M_H$ and $M_V$ denote the horizontal and vertical component of the geomagnetic field vector norm, $M_{sx0}$, $M_{sy0}$, and $M_{sz0}$ denote the outputs of the magnetic sensor without the coning motion, and $\psi_0$, $\theta_0$, and $\gamma_0$ are the magnetic yaw angle, magnetic pitch angle, and roll angle without the coning motion, respectively. Within the range of conventional artillery, the variation of the geomagnetic field vector norm and magnetic declination are quite small, so $M_H$ and $M_V$ can be regarded as constants. When the spinning projectile flies in coning motion, the attitude angles need to be corrected by (2)

$$
\begin{cases}
\psi = \psi_0 + \delta \sin 2\pi f t \\
\theta = \theta_0 + \delta \cos 2\pi f t , \\
\gamma = \gamma_0
\end{cases}
\tag{2}
$$

where $\psi$, $\theta$, and $\gamma$ denote the yaw angle, pitch angle, and roll angle with the coning motion, $\delta$ is the taper angle, and $f$ is the coning motion frequency, respectively.

The tri-orthogonal geomagnetic attitude measurement method of the spinning projectile includes the cross ratio method, integral ratio method, derivative ratio method and so on. The characteristics of magnetic sensor outputs selected by these methods are different, as shown in Table 1.

Table 1. Characteristics required by tri-orthogonal geomagnetic attitude measurement methods.

| Measurement Method | Characteristics |
|---|---|
| Cross Ratio Method | Ratio between the Intersections of Outputs of $y$ and $z$ Axes and the Output of $x$ Axis |
| Integral Ratio Method | Integration between 0-value Points of Outputs of $y$ and $z$ Axes |
| Derivative Ratio Method | Derivative at 0-value Points of Outputs of $y$ and $z$ Axes |

However, when there is large interference in the output signals, no matter which algorithm is used, there will be two problems. One is that the position of characteristic points will be offset due to noise, and the other is that the solution error of characteristics will be generated due to noise, as shown in Fig. 1.

In order to reduce the influence of noise on the tri-orthogonal geomagnetic attitude measurement method, the actual output signals of the magnetic sensor can be fitted to the standard output signals based on the tri-orthogonal geomagnetic equations. In this case, not only the position
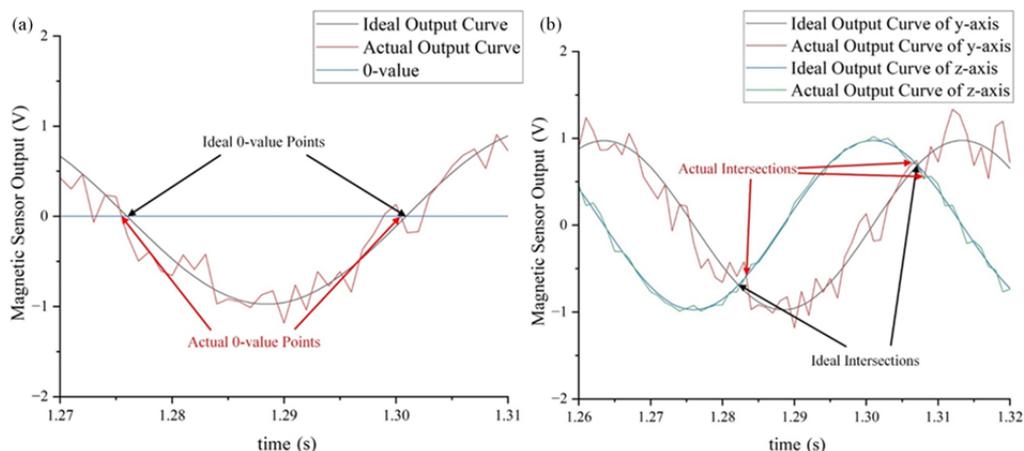
Fig. 1. Influence of noise on characteristic points with influence of noise on 0-value position (a) or influence of noise on intersection position (b).

of characteristic points can be obtained quickly and directly by fitting the signals, but also the characteristic values can be directly calculated according to the fitted parameters, completely omitting the complex signal processing such as denoising and filtering.

## 3. Improved particle swarm optimization fitting algorithm

*Particle swarm optimization* (PSO) is an algorithm with many advantages, such as simple steps, fewer parameters and fast convergence. In this study, an improved PSO algorithm is used to transform data fitting into nonlinear function optimization, and the results can be obtained simply and quickly through an indirect way.

Each particle in the PSO algorithm is a *D* dimension vector, which is a search individual in the optimization space. The particle position in each iteration can be regarded as a candidate solution, and the flight process of the particle is the search process. The particle speed can be adjusted in real time based on the optimal position of a single particle and all particles in the iterative process. A particle has only two attributes: speed and position. Speed represents the velocity of particle motion, and position represents the direction of particle optimization. The optimal solution in the optimization process of a single particle is the individual extreme value, and the optimal solution in the optimization process of all particles is the current global optimal solution. In each iteration, the particle speed, position and optimal solution are continuously updated, and the optimal solution is obtained when the convergence is finally completed or the termination condition is met [21–25]. The subsequent steps of the PSO algorithm are as follows:

1. Initialize
   First, set the termination condition. The maximum number of iterations is usually selected based on experience. Take initial condition randomly in the speed range and search space, and set the number of arguments of the objective function, particle speed range $[V_{\min}, V_{\max}]$, position range $[x_{\min}, x_{\max}]$ and particle number $N$.
2. Individual extremum and global optimal solution
   Define the fitness function and the selection principle of the optimal solution. The global optimal solution obtained in each iteration needs to be updated after comparing with the historical global optimal solution.

3. Update speed and position

   Among the $N$ particles in the $D$ dimension space, the position and speed of the $i-$th particle are expressed as $x_i = [x_{i1}, x_{i2}, \ldots, x_{id}]$ and $V_i = [V_{i1}, V_{i2}, \ldots, V_{id}]$, respectively. Update the speed and position according to (3) and (4)

$$V_{id}(k+1) = \omega V_{id}(k) + C_1 r_1(P_{id}(k) - x_{id}(k)) + C_2 r_2(G_{id}(k) - x_{id}(k)), \tag{3}$$

$$x_{id}(k+1) = x_{id}(k) + V_{id}(k+1), \tag{4}$$

   where $i = 1, 2, \cdots, N$, $d = 1, 2, \cdots, D$, $\omega$ is the inertia weight factor, which is usually a constant in the conventional PSO algorithm. $k$ is the current iteration number. $C_1$ and $C_2$ are learning factors, generally 2. $r_1$ and $r_2$ are random numbers evenly distributed between 0 and 1. $P_{id}(k)$ and $G_{id}(k)$ are the fitness and global fitness of the $i$-th particle, respectively.

During the fitting, the fitness function can be constructed by the least square method, and the problem can be converted into optimization of obtaining the minimum value of the function, as shown in (5)

$$M_i = \min \left[ \sqrt{(\boldsymbol{M}_s - \boldsymbol{M}_t)^{\mathrm{T}} (\boldsymbol{M}_s - \boldsymbol{M}_t)} \right], \tag{5}$$

where $M_i$ is the fitness, $\boldsymbol{M}_t$ is the actual output of the magnetic sensor, and $\boldsymbol{M}_s$ is the ideal output of the magnetic sensor.

Combining (1) and (2), the estimated parameters of the attitude measurement outputs of the spinning projectile are initial attitude angles $\psi_i = \psi(0)$, $\theta_i = \theta(0)$, $\gamma_i = \gamma(0)$, taper angle $\delta$ and coning motion frequency $f$. The initial roll angle is defined manually, and is usually taken as 0 for convenience. In addition, the roll angle $\gamma$ should be replaced with a function of time $\gamma = 2\pi f_0 t$, where $f_0$ is the roll angle frequency. Then there are 5 parameters to be estimated in this case, namely $\psi_0, \theta_0, f_0, \delta, f$.

In the actual situation, all physical quantities have initial values and constraints. When fitting the tri-orthogonal magnetic sensor attitude measurement outputs, the constraint conditions should be set according to (6)

$$\begin{cases} 0 \leq \psi_l < \psi_i < \psi_h < 2\pi \\ -\pi/2 \leq \theta_l < \theta_i < \theta_h \leq \pi/2 \\ f_0 > 0 \\ \delta > 0 \\ f > 0 \end{cases}, \tag{6}$$

where $\psi_h$ and $\psi_l$ are the upper and lower limit of magnetic yaw angle coarse alignment, $\theta_h$ and $\theta_l$ are the upper and lower limit of magnetic pitch angle coarse alignment. According to the stability theory of the spinning projectile, its roll angle frequency is proportional to the coning motion frequency, which is related to the length-diameter ratio of the projectile, and the proportion is $m$. As an important structural parameter of the projectile, the length-diameter ratio of the projectile is a known quantity. Assuming that the proportion range estimated by the projectile length-diameter ratio is $m_l \sim m_h$, (6) can be upgraded to (7)

$$\begin{cases} 0 \leq \psi_l < \psi_i < \psi_h < 2\pi \\ -\pi/2 \leq \theta_l < \theta_i < \theta_h \leq \pi/2 \\ 0 < f/m_h < f_0 < f/m_l \\ \qquad \delta > 0 \\ \qquad f > 0 \end{cases} \qquad . \tag{7}$$

In PSO, the inertia weight factor $\omega$ is a parameter that affects the exploration ability of the algorithm. The higher is the value, the stronger is the global search ability. And contrarily, the smaller is the value, the stronger is the local search ability. Because of the strong nonlinearity of the tri-orthogonal magnetic sensor outputs, the fitness function constructed by (5) has a lot of local optimal values. This raises problems such as spending a too long time to search for the optimal value, easy falling into the local optimum, and being unable to select the optimal value. In order to give consideration to the global and local search ability of the algorithm, the inertia weight factor should be gradually reduced during the whole optimization process, so that the iterative process can quickly converge to the interval of the optimal solution.

The adaptive adjustment strategy is used to dynamically adjust the inertia weight of particles, which can make it take a larger value in the early stage and improve the activity of the particles. On the contrary, the weight can be reduced at a later stage, so that the particles can converge near the elite particles and close to the global optimal solution. For convenience, the following strategies can be used to adjust the weights.

1. Reduce with the linear function
2. Reduce with the concave quadratic function
3. Reduce with the convex quadratic function
4. Reduce with the tangent function
5. Reduce with the arctangent function

## 4. Experiment and results

The experimental equipment described in [6] is used to verify the improved PSO algorithm proposed in this study, as shown in Fig. 2.



Fig. 2. Semi-physical experimental device.

First, the turntable should be adjusted so that it can carry the semi-physical device to make coning motion according to the following parameters

$$\begin{cases} \psi_i = 30° \\ \theta_i = 80° \\ f_0 = 20 \text{ Hz} \\ \delta = 5° \\ f = 2 \text{ Hz} \end{cases} . \tag{8}$$

According to (1), the outputs of y-axis and z-axis magnetic sensors are affected by more parameters to be estimated, and the outputs of y-axis and z-axis are only different in phase. Therefore, the output of y-axis is taken as an example, and its actual measured normalized output is shown in Fig. 3.
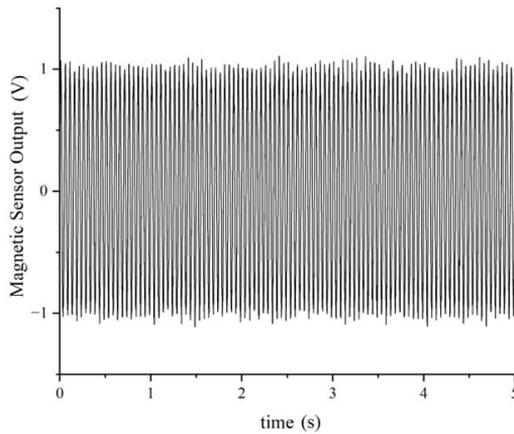


Fig. 3. Actual output curve of *y*-axis.

From Fig. 3, it can be found that the information about the size of taper angle and the coning motion frequency almost disappeared in the noise.

Then the constraints should be set. In other commonly used attitude measurement methods, such as inertial attitude measurement, it is necessary to obtain more accurate initial states through initial alignment. However, the fitting method proposed in Section 3 of this study does not need such accurate initial states. The initial state values can be set in a quite large range It even can be directly determined with the naked eye. In addition, assuming $m = 10 \pm 0.4$, the fitting constraints are shown in (9)

$$\begin{cases} 0° < \psi_i < 45° \\ 45° < \theta_i < 180° \\ f_0 > 0 \\ \delta > 0 \\ 0 < f_0/10.4 < f < f_0/9.6 \end{cases} . \tag{9}$$

The commonly used fixed weight and linear weight reduction strategies in PSO algorithm, and the four improved weight strategies are adopted to solve the fitness function. The maximum number of iterations is set to 300, the number of particles is 1000, the fixed weight factor is set to 0.2, and the weights of the improved methods are reduced from 0.8 to 0.2 according to their respective function rules.

$$\begin{cases} \omega_1 = 0.2 \\[4pt] \omega_2 = 0.8 - 0.002k \\[4pt] \omega_3 = -\dfrac{3k^2}{449995} + \dfrac{359999}{449995} \\[8pt] \omega_4 = \dfrac{3k^2}{447005} - \dfrac{360k}{89401} + \dfrac{359401}{447005} \\[8pt] \omega_5 = \dfrac{-3\tan\left[8\left(k - 149.5\right)\pi/2700\right]}{10\tan\left(4\pi/9\right)} + 0.5 \\[8pt] \omega_6 = -\dfrac{3\arctan\left[(k - 149.5)/3\right]}{5\pi} + 0.5 \end{cases}, \tag{10}$$

where $k$ is the number of iterations.

Figure 4 shows the weight changes of different improved strategies.
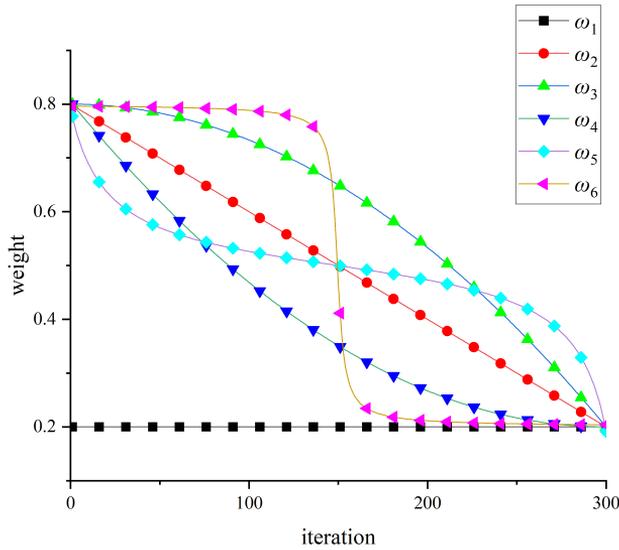


Fig. 4. Schematic diagram of weight changes.

The semi-physical device records the data measured by sensors during the motion process and performs the fitting calculations offline. The fitting results are shown in Table 2 to Table 7, and the solutions that do not get the global optimum are marked with "*". After multiple iterations in each fitting test, the fitted parameters will converge to a fixed value, and the convergence position in the tables is the number of iterations at the convergence. To compare the fitting effects of different weight optimization strategies, the same dataset is used for fitting.

The differential evolution algorithm exhibits strong robustness in solving non convex, multimodal, and nonlinear function optimization problems, and is especially adept at handling multivariate function optimization problems. So, the differential evolution algorithm with an adaptive mutation operator is selected to compare with the proposed improved PSO algorithm (Table 8).

Table 2. Fitting results for the fixed weight factor.

| Fitting times | $\psi_i$ (°) | $\theta_i$ (°) | $f_0$ (Hz) | $\delta$ (°) | $f$ (Hz) | Convergence position |
|---|---|---|---|---|---|---|
| 1 | 29.9703 | 80.0966 | 19.9999 | 5.3176 | 2.0002 | 39 |
| 2 | 29.4504 | 79.2840 | 20.0002 | 4.9184 | 1.9969 | 93 |
| 3 | 29.9278 | 80.1011 | 20.0000 | 5.0534 | 1.9991 | 37 |
| 4 | 29.9008 | 80.2412 | 19.9999 | 5.1431 | 2.0001 | 143 |
| 5* | 39.2365 | 82.0403 | 20.0000 | 2.1255 | 2.0682 | 239 |
| 6* | 0 | 99.5424 | 19.9958 | 3.1294 | 2.0678 | 35 |
| 7 | 30.3216 | 79.8315 | 20.0001 | 4.9652 | 2.0008 | 47 |
| 8* | 45.0000 | 82.5914 | 20.0003 | 4.0088 | 2.0065 | 70 |
| 9 | 29.3786 | 79.9269 | 20.0000 | 5.1204 | 2.0005 | 28 |
| 10* | 0 | 99.6112 | 19.9959 | 3.7521 | 2.0678 | 50 |

Table 3. Fitting results for the linear weight factor.

| Fitting times | $\psi_i$ (°) | $\theta_i$ (°) | $f_0$ (Hz) | $\delta$ (°) | $f$ (Hz) | Convergence position |
|---|---|---|---|---|---|---|
| 1 | 29.5875 | 79.9849 | 19.9999 | 4.9389 | 1.9992 | 243 |
| 2* | 0 | 99.4254 | 19.9958 | 3.1856 | 2.0678 | 121 |
| 3* | 45.0001 | 82.4429 | 20.0003 | 3.7128 | 2.0090 | 171 |
| 4 | 28.6651 | 79.4177 | 20.0000 | 5.0649 | 1.9981 | 269 |
| 5 | 30.1441 | 80.0197 | 20.0001 | 4.9111 | 2.0000 | 155 |
| 6 | 29.1025 | 79.9667 | 19.9999 | 5.0345 | 1.9991 | 184 |
| 7 | 30.1184 | 79.9681 | 20.0001 | 4.7954 | 2.0012 | 132 |
| 8 | 30.1239 | 79.9584 | 20.0000 | 5.0877 | 2.0022 | 124 |
| 9 | 30.5661 | 80.1467 | 19.9999 | 5.0952 | 2.0020 | 227 |
| 10 | 25.6855 | 78.7299 | 19.9999 | 5.1224 | 2.0018 | 285 |

Table 4. Fitting results for the concave quadratic weight factor.

| Fitting times | $\psi_i$ (°) | $\theta_i$ (°) | $f_0$ (Hz) | $\delta$ (°) | $f$ (Hz) | Convergence position |
|---|---|---|---|---|---|---|
| 1 | 30.4185 | 79.9689 | 20.0000 | 4.9205 | 1.9995 | 272 |
| 2 | 29.7814 | 80.0028 | 20.0000 | 4.8883 | 2.0019 | 195 |
| 3 | 29.6732 | 79.7825 | 20.0001 | 5.0264 | 2.0011 | 284 |
| 4 | 30.5923 | 80.2041 | 20.0000 | 5.0006 | 2.0017 | 265 |
| 5* | 0.0000 | 99.2765 | 19.9959 | 3.2757 | 2.0678 | 195 |
| 6 | 30.5432 | 79.8731 | 20.0001 | 5.0275 | 2.0025 | 235 |
| 7 | 31.5388 | 80.4662 | 20.0000 | 4.8013 | 2.0039 | 265 |
| 8* | 0.0000 | 80.0772 | 19.9959 | 0.0000 | 2.0623 | 290 |
| 9 | 31.5860 | 80.1365 | 20.0002 | 4.7041 | 2.0009 | 231 |
| 10 | 29.7223 | 79.9971 | 19.9999 | 5.1213 | 2.0000 | 243 |

Table 5. Fitting results for the convex quadratic weight factor.

| Fitting times | $\psi_i$ (°) | $\theta_i$ (°) | $f_0$ (Hz) | $\delta$ (°) | $f$ (Hz) | Convergence position |
|---|---|---|---|---|---|---|
| 1* | 0.0000 | 80.0291 | 19.9959 | 7.0361 | 1.9489 | 291 |
| 2 | 31.9462 | 80.4688 | 20.0000 | 4.9832 | 2.0019 | 211 |
| 3 | 29.0827 | 80.0553 | 19.9999 | 4.9563 | 1.9983 | 110 |
| 4 | 31.6281 | 80.1762 | 20.0001 | 4.9812 | 2.0034 | 153 |
| 5 | 28.9830 | 79.5413 | 20.0000 | 4.8768 | 1.9968 | 141 |
| 6* | 0.0000 | 100.0791 | 19.9958 | 3.0577 | 2.0678 | 84 |
| 7 | 30.8577 | 80.1553 | 20.0000 | 4.9351 | 1.9993 | 158 |
| 8 | 29.9823 | 79.8880 | 20.0000 | 5.0567 | 1.9983 | 172 |
| 9 | 29.7722 | 79.9363 | 19.9999 | 5.1987 | 1.9979 | 138 |
| 10 | 30.5448 | 79.9819 | 20.0001 | 4.9716 | 2.0002 | 189 |

Table 6. Fitting results for the tangent weight factor.

| Fitting times | $\psi_i$ (°) | $\theta_i$ (°) | $f_0$ (Hz) | $\delta$ (°) | $f$ (Hz) | Convergence position |
|---|---|---|---|---|---|---|
| 1 | 24.4093 | 81.3644 | 19.9988 | 5.0721 | 2.0403 | 81 |
| 2 | 31.3757 | 80.4418 | 20.0001 | 4.8237 | 2.0003 | 94 |
| 3* | 43.4362 | 82.5611 | 20.0001 | 3.9973 | 2.0089 | 83 |
| 4 | 32.2897 | 80.9197 | 19.9999 | 5.0543 | 1.9976 | 98 |
| 5 | 31.1643 | 80.2741 | 20.0000 | 4.9964 | 1.9990 | 106 |
| 6 | 29.9912 | 79.6465 | 20.0002 | 5.0349 | 2.0014 | 130 |
| 7 | 31.1679 | 81.1749 | 19.9996 | 4.9057 | 2.0036 | 93 |
| 8 | 30.7873 | 79.8559 | 20.0002 | 4.7361 | 2.0010 | 87 |
| 9 | 31.6597 | 80.3501 | 20.0001 | 5.0828 | 2.0019 | 93 |
| 10 | 28.8787 | 79.7702 | 19.9999 | 5.3184 | 2.0003 | 120 |

Table 7. Fitting results for the arctangent weight factor.

| Fitting times | $\psi_i$ (°) | $\theta_i$ (°) | $f_0$ (Hz) | $\delta$ (°) | $f$ (Hz) | Convergence position |
|---|---|---|---|---|---|---|
| 1 | 29.7243 | 79.8972 | 20.0001 | 5.0384 | 1.9984 | 198 |
| 2 | 29.6049 | 79.7290 | 20.0001 | 5.0981 | 2.0007 | 220 |
| 3 | 31.3681 | 80.2188 | 20.0002 | 4.8864 | 1.9994 | 177 |
| 4 | 30.6718 | 79.9434 | 20.0001 | 4.8412 | 2.0007 | 179 |
| 5 | 30.0270 | 80.0158 | 19.9999 | 4.9662 | 1.9998 | 223 |
| 6 | 30.7264 | 79.8772 | 20.0001 | 4.9464 | 2.0011 | 179 |
| 7 | 30.7567 | 80.0707 | 20.0001 | 4.9888 | 1.9997 | 189 |
| 8 | 30.4703 | 80.0085 | 20.0000 | 4.7779 | 1.9970 | 185 |
| 9 | 30.9410 | 80.4645 | 19.9999 | 5.1159 | 2.0014 | 187 |
| 10 | 31.0908 | 80.4559 | 19.9999 | 5.1015 | 2.0019 | 214 |

Table 8. Fitting results of the differential evolution algorithm with an adaptive mutation operator.

| Fitting times | $\psi_i$ (°) | $\theta_i$ (°) | $f_0$ (Hz) | $\delta$ (°) | $f$ (Hz) |
|---|---|---|---|---|---|
| 1 | 31.8335 | 81.3199 | 19.9994 | 4.0222 | 2.0261 |
| 2 | 35.4177 | 81.6571 | 20.0002 | 4.7767 | 2.0055 |
| 3 | 26.0483 | 78.8646 | 19.9998 | 5.7468 | 1.9785 |
| 4 | 22.5028 | 77.1077 | 20.0002 | 5.1273 | 1.9740 |
| 5 | 31.2693 | 77.3764 | 20.0019 | 2.7498 | 1.9970 |
| 6 | 24.8903 | 77.6863 | 20.0002 | 5.2514 | 1.9944 |
| 7 | 21.0085 | 75.5578 | 19.9992 | 4.5625 | 1.9772 |
| 8 | 31.9449 | 80.8591 | 19.9998 | 4.8565 | 1.9994 |
| 9 | 41.4907 | 82.6164 | 19.9999 | 4.3217 | 2.0048 |
| 10 | 33.6637 | 83.4166 | 19.9982 | 3.3272 | 2.0102 |

## 5. Discussion

It can be seen from the fitting data that the PSO algorithm and its improved algorithms have a relatively good fitting effect under the condition of uncertain initial state and loose constraints. Because the particles move randomly, the convergence positions of some data are far from the convergence position of other data in the same group, but most of them are close to each other. The PSO algorithm can converge to a local optimum at a high speed due to its small weight factor, but it is difficult to ensure that the point is the global optimum, so there is a high probability that accurate fitting results cannot be obtained. The convex quadratic improved algorithm and the tangent improved algorithm have a fast rate of inertia weight factor reduction in the early stage, so they converge fast. The tangent improved algorithm has a long time to maintain at the middle weight, so the fitting results are more stable than the convex quadratic improved algorithm. The other three improved algorithms search for the global optimum at the early stage. They converge slowly because of the slow reduction of inertia weight factor. Among all of the improved algorithms, the tangent improved algorithm has high speed and a relatively good stability, while the arctangent improved algorithm has the highest stability. These two algorithms have high application values under loose constraints, but also have the disadvantage of complex calculation of the inertia weight factor reduction function. The other improved algorithms can easily determine the inertia weight factor reduction function and can also improve their fitting stability when the initial states are relatively accurate.

Compared to the differential evolution algorithm with an adaptive mutation operator, the improved PSO algorithm has a higher accuracy. This is because the differential evolution algorithm may have a low solving accuracy when the complexity of the problem to be solved is high. In addition, the differential evolution algorithm needs to set upper and lower limits for each parameter to be solved, which is equivalent to strengthening constraints, compared to the proposed algorithm. Therefore, the improved PSO algorithm has more advantages in solving similar problems.

## 6. Conclusions

Because it is difficult to determine the position of characteristic points and the solution results are significantly biased when the characteristics are obtained from the measured outputs of the magnetic sensor under the coning motion directly, an improved PSO algorithm to get the approximate standard outputs by data fitting is proposed in this study. By comparing different improved strategies,

the advantages, disadvantages and applicability of each strategy are analysed. This method can obtain quite accurate estimated parameters under loose constraints and initial conditions. It can also provide a stable and accurate supervised learning algorithm in a wide range of similar applications.

Compared to the rate of change in roll angle and the rate of change in pitch angle and yaw angle caused by the coning motion, the rate of change in pitch angle caused by the trajectory is much smaller. Therefore, in the current tri-orthogonal geomagnetic attitude measurement model, the pitch angle centre value is considered constant in a single calculation. The pitch angle obtained from each solution is treated as the initial condition for the next iteration. The attitude solution model should update if the trajectory model is known and this will bring more undetermined parameters and constraints. Because of the considerable computational resources required for the improved PSO algorithm, upgrading the attitude measurement model may lead to overfitting and require more computation time. In subsequent research, further consideration should be given to improving the fitting strategy of the improved PSO algorithm, so it can have a better fitting efficiency and effect for more complex models.

## References

[1] He, Z., Bu, X., Yang, H., & Song, Y. (2021). Interacting multiple model cubature Kalman filter for geomagnetic/infrared projectile attitude measurement. *Measurement*, *174*(1), 109077. https://doi.org/10.1016/j.measurement.2021.109077

[2] Wang, W., Meng, G., Liu, J., Wang, M., Gao, Z., Mu, L., & Zhang, S. (2018, December). Integrated navigation method based on inertial and geomagnetic information fusion. *Optical Sensing and Imaging Technologies and Applications* (Vol. 10846, pp. 278–292). SPIE. https://doi.org/10.1117/12.2504356

[3] Xiang, C., Bu, X. Z., & Yang, B. (2014). Three different attitude measurements of spinning projectile based on magnetic sensors. *Measurement*, *47*, 331–340. https://doi.org/10.1016/j.measurement.2013.09.002

[4] Yu, J., Bu, X., Xiang, C., & Yang, B. (2017). Spinning projectile's attitude measurement using intersection ratio of magnetic sensors. *Proceedings of the Institution of Mechanical Engineers, Part G: Journal of Aerospace Engineering*, *231*(5), 866–876. https://doi.org/10.1177/0954410016644628

[5] Xu, M., Bu, X., He, Z., & Han, W. (2019). Integral ratio method for the geomagnetic attitude measurement of spinning projectiles. *Journal of Harbin Engineering University*, *40*(06), 1163–1168. https://doi.org/10.11990/jheu.201804009

[6] He, Z., Bu, X., Yang, H., & Song, Y. (2021). Derivative ratio attitude solution algorithm of tri-orthogonal magnetic sensor for spinning projectile. *Measurement*, *186*, 110228. https://doi.org/10.1016/j.measurement.2021.110228

[7] Chughtai, F. A., Masud, J., & Akhtar, S. (2019). Unsteady aerodynamics computation and investigation of Magnus effect on computed trajectory of spinning projectile from subsonic to supersonic speeds. *The Aeronautical Journal*, *123*(1264), 863–889. https://doi.org/10.1017/aer.2019.32

[8] Lijin, J., & Jothi, T. J. S. (2018). Aerodynamic characteristics of an ogive-nose spinning projectile. *Sādhanā. Academy Proceedings in Engineering Sciences 43*, 1-8.

[9] Norris, J., Hameed, A., Economou, J., & Parker, S. (2020). A review of dual-spin projectile stability. *Defence Technology*, *16*, 1–9. https://doi.org/10.1016/j.dt.2019.06.003

[10] Li, D., & Bu, X. Z. (2010). Roll angle measurement of spinning projectile based on non-orthogonal magnetic sensors. *Acta Armamentarii*, *31*(10), 1316–1321.

[11] Yu, X., Xiao, C., Liu, S., Zong, Q., Qu, Y., Chen, H., Zou, H., Shi, W., Wang, Y., Chen, A., Song, S., Gao, S., & Shao, S. (2020). Calibration of AC vector magnetometer based on ellipsoid fitting. *IEEE Transactions on Instrumentation and Measurement*, *70*, 1–6. https://doi.org/10.1109/TIM.2020.3014980

[12] Li, L., & Huang, J. (2018). Recursive of Least Square Based Online Calibration Method in Geomagnetic Detection. *MATEC Web of Conferences* (Vol. 232, p. 04087). EDP Sciences.

[13] Sun, W., Yang, Y. H., & Wang, Y. (2018). Research on Error Correction of Magnetometer Based on Ellipsoid Fitting [J]. *Chinese Journal of Sensors and Actuators*, *31*(09), 1373–1376. https://doi.org/10.3969/j.issn.1004-1699.2018.09.013

[14] Li, X., Song, B., Wang, Y., Niu, J., & Li, Z. (2018). Calibration and alignment of tri-axial magnetometers for attitude determination. *IEEE Sensors Journal*, *18*(18), 7399–7406. https://doi.org/10.1109/JSEN.2018.2859832

[15] Farhangian, F., Bilel, S., Farhangian, F., & Landry Jr., R. (2021). A magnetometer calibration method using single-axis motion trajectory and unscented Kalman filter for body motion capture applications. *International Journal of Sensors and Sensor Networks*, *9*(1), 1. https://doi.org/10.11648/J.IJSSN.20210901.11

[16] Crassidis, J. L., & Cheng, Y. (2021). Three-axis magnetometer calibration using total least squares. *Journal of Guidance, Control, and Dynamics*, *44*(8), 1410–1424. https://doi.org/10.2514/1.G005305

[17] Lu, J. (2016). A fault tolerant, data fusion system for navigation applications to a ducted fan VTOL UAV. *Open Access Master's Report*, Michigan Technological University, 2016. https://doi.org/10.37099/mtu.dc.etdr/98

[18] Zhou, Z., Wang, L., Fu, J., & An, L. (2021, July). Aerodynamic parameters identification for high-spinning projectile based on geomagnetic data. *2021 40th Chinese Control Conference* (*CCC*) (pp. 1236–1242). IEEE. https://doi.org/10.23919/CCC52363.2021.9549442

[19] Deng, Z., Wang, J., Liang, X., & Liu, N. (2020). A coupling method of geomagnetic aided inertial attitude errors. *IEEE Sensors Journal*, *20*(23), 14282-14289. https://doi.org/10.1109/JSEN.2020.3007210

[20] Cuenca, A., & Moncayo, H. (2022). Machine learning application to estimation of magnetospheric contributions for geomagnetic-based navigation. *AIAA SCITECH 2022 Forum* (p. 1714). https://doi.org/10.2514/6.2022-1714

[21] Wang, H., Jin, Y., & Doherty, J. (2017). Committee-based active learning for surrogate-assisted particle swarm optimization of expensive problems. *IEEE Transactions on Cybernetics*, *47*(9), 2664–2677. https://doi.org/10.1109/TCYB.2017.2710978

[22] Bui, D. T., Bui, Q. T., Nguyen, Q. P., Pradhan, B., Nampak, H., & Trinh, P. T. (2017). A hybrid artificial intelligence approach using GIS-based neural-fuzzy inference system and particle swarm optimization for forest fire susceptibility modeling at a tropical area. *Agricultural and Forest Meteorology*, *233*, 32–44. https://doi.org/10.1016/j.agrformet.2016.11.002

[23] Ding, Y., Cheng, L., Pedrycz, W., & Hao, K. (2015). Global nonlinear kernel prediction for large data set with a particle swarm-optimized interval support vector regression. *IEEE Transactions on Neural Networks and Learning Systems*, *26*(10), 2521–2534. https://doi.org/10.1109/TNNLS.2015.2426182

[24] Su, Y. X., & Chi, R. (2017). Multi-objective particle swarm-differential evolution algorithm. *Neural Computing and Applications*, *28*, 407–418. https://doi.org/10.1007/s00521-015-2073-y

[25] Tang, B., Zhanxia, Z., & Luo, J. (2017). A convergence-guaranteed particle swarm optimization method for mobile robot global path planning. *Assembly Automation*, *37*(1), 114–129. https://doi.org/10.1108/AA-03-2016-024

**Zilu He** received his B.Sc. and M.Sc. degrees in measurement & control technology and instrument engineering from Nanjing University of Science and Technology in 2014 and 2017, respectively, and his Ph.D. degree in instrument science and technology from the same university in 2022. He is currently an engineer at Shanghai Electro-Mechanical Engineering Institute. His current research interest are dynamic measurement, signal processing and fault diagnosis.
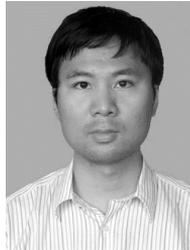
**Xin Chen** graduated from Harbin Institute of Technology in 2012, majoring in communication and information systems. He is currently a Senior Engineer at Shanghai Electro-Mechanical Engineering Institute. His current research interest is telemetry system design.

**Qi Liang** received his M.Sc. degree in optical engineering from Nanjing University of Science and Technology in 2013. He is currently a Senior Engineer at Shanghai Electro-Mechanical Engineering Institute. His current research interest is measurement system design.

**Miaomiao Xu** received his B.Sc. and Ph.D. degrees in instrument science and technology from Nanjing University of Science and Technology in 2014 and 2019. He is currently an associate professor at the School of Information Science and Technology, Nantong University. His research interests focus on signal processing, integrated navigation and instrumental science and technology.

**Yiji Liu** obtained his M.Sc. degree in management from the University of Leicester, UK, in 2011. He is currently a Senior Engineer at Shanghai Electro-Mechanical Engineering Institute. His research activity focuses on project management in measurement and control system design.

**Xiongzhu Bu** is a professor at Nanjing University of Science and Technology (NJUST). He received his B.Sc. and M.Sc. degrees in dynamic measurement from NJUST in 1988 and 1990, respectively, and his Ph.D. degree in dynamic measurement from the same university in 1993. His current research interests include sensor technology, dynamic measurements, digital signal processing, smart instrumentation design and application.

**Yundong He** graduated from East China Normal University in 2010, majoring in circuits and systems. He is currently a Senior Engineer at Shanghai Electro-Mechanical Engineering Institute. His current research interest is telemetry system design.